Journal of Catalysis 275 (2010) 228–235

Contents lists available at ScienceDirect

Journal of Catalysis

journal homepage: www.elsevier.com/locate/jcat

Ni on alumina-coated cordierite monoliths for in situ generation of CO-free H_2 from ammonia

Carlos Plana [a], Sabino Armenise [a], Antonio Monzón [b], Enrique García-Bordejé [a,*]

[a] Instituto de Carboquimica (C.S.I.C.), Miguel Luesma Castán 4, 50018 Zaragoza, Spain
[b] Institute of Nanoscience of Aragon, Department of Chemical and Environmental Engineering, University of Zaragoza, 50018 Zaragoza, Spain

ARTICLE INFO

Article history:
Received 26 May 2010
Revised 19 July 2010
Accepted 29 July 2010
Available online 15 September 2010

Keywords:
Monolith
Hydrogen
Ammonia
Nickel

ABSTRACT

We present here the testing results in NH_3 decomposition of a catalytic structured reactor consisting of a cordierite monolith coated with a catalyst layer of well-dispersed Ni on mesoporous γ-alumina. The catalyst is low cost, stable and exhibits high activity, achieving complete conversion of pure NH_3 at a temperature as low as 873 K. Notably, the conversion is significantly higher when the catalyst is in the form of monolith than in a packed bed of the same catalyst in the form of particles smaller than 200 μm, achieving total NH_3 conversion at 100 K lower temperature. These results along with the process intensification derived from the use of monolithic catalyst make this catalyst a promising candidate for in situ H_2 generation from ammonia to feed fuel cells in vehicles or industry.

1. Introduction

The drive for reducing emission levels in automobile exhaust and for developing efficient small-scale power generation units (<5 kW) has resulted in a renewed interest in hydrogen generation to power proton exchange membrane (PEM) fuel cells. These fuel cells require a supply of carbon monoxide-free hydrogen gas (<50 ppm) to the anode in order to avoid poisoning of the anode catalyst. Because the transportation costs of H_2 are about double than the cost of hydrogen produced by conventional steam reforming [1], local production of hydrogen (on-site) is considered to be a viable option, particularly if the size of the hydrogen generation unit can be tailored to satisfy the needs of specific power requirements.

Due to the necessity of a virtually carbon monoxide-free hydrogen feed, integrated fuel cell processes that use hydrocarbon fuels are rather complex and require multiple processing steps such as desulfurization, water gas shift, methanation and preferential oxidation to reduce carbon monoxide levels in the reformer outlet gas. Consequently, hydrogen from a single-step source like ammonia decomposition has been postulated as an alternative to hydrocarbon fuels for small-scale fuel cell applications. Ammonia has a high hydrogen content (17.7 wt.%), and it can be conveniently stored in liquid form at room temperature and low pressure (6 atm). Thus, the safety issues concerning its storage and handling are well established. Recently, it has been reported that ammonia can be also stored as solid compounds named Hydrammines™ [2]. More importantly, the product stream (hydrogen/nitrogen) is CO-free and unconverted ammonia can be reduced to less than 200 ppb by means of a suitable adsorbent [3].

The design of catalysts for ammonia decomposition is an interesting challenge, since this reaction can be used for on-site hydrogen generation in proton exchange membrane fuel cells [4]. Recently, several groups have investigated the reaction of ammonia decomposition based on the catalyst developed previously for the ammonia synthesis. Underpinned by ammonia synthesis results [5,6], most of the catalysts tested for ammonia decomposition are based on noble metals, especially ruthenium on different supports such as alumina [7–9], graphitized carbon [10,11], carbon nanotubes [12] and nitrogen-doped carbon nanotubes [13–15] and also ruthenium catalyst with different promoters [15,16]. However, it is still challenging to explore a highly active and economical NH_3 decomposition catalyst to meet the strict requirements of a "green" energy system based on hydrogen. There has been a few works in which the noble metal catalyst is substituted by other more economic active phases such as vanadium nitride [17], nickel [18,19], nickel–platinum [20] or iron–cobalt nanoparticles [21]. It is reported that although Ru is the most active catalyst, the activity of nickel is very close [18,19]. Since the catalyst is aimed for a widespread application such as the generation of H_2 for vehicles, the cost of the catalyst is crucial.

From the point of view of applicability for on-site production, it is convenient to have the catalyst in the form of structured reactor. The small scales of microstructured devices have inherent advantages, including high heat and mass transfer coefficients and high

* Corresponding author. Fax: +34 976733318.
E-mail address: jegarcia@icb.csic.es (E. García-Bordejé).

0021-9517/$ - see front matter © 2010 Elsevier Inc. All rights reserved.
doi:10.1016/j.jcat.2010.07.026

surface area to volume ratios. Vlachos et al. [22] demonstrated by CFD simulation that microreactors led to higher NH_3 conversions compared with that of tubular reactor and CSTR. As catalytic reactors, Ru on graphite-coated silica microreactors [10], on silicon carbide [23] and on alumina [8] micoreactors have been used for this reaction. Cordierite monoliths are structured reactors with multiple channels of several hundreds of microns diameter. Monoliths have uniform flow distribution and low pressure drop which is crucial for the energy-efficiency of the process. Furthermore, they are commercially available, and they can withstand high temperatures and their coating with catalyst layer is a mature technology [24].

Here, we have coated cordierite monoliths with mesoporous γ-alumina. Subsequently, we have dispersed Ni by electrostatic adsorption. This catalytic structured reactor has been thoroughly characterized by TEM, XRD, N_2 phisisorption and TPR, and it has been tested in NH_3 decomposition for in situ H_2 generation under realistic conditions such as pure NH_3 feed and high space velocity. We have compared the behaviour of the catalysts varying the configuration, i.e. monolith or packed beds, and experimental conditions such as different NH_3 concentrations and flow rates. Finally, the results have been discussed and put into perspective with other catalysts in the open literature.

2. Experimental

2.1. Catalyst preparation

Cordierite monoliths (from Corning, 10 mm diameter, 65 mm length, 400 cpsi, ca. 2.4 g) were washcoated with alumina by dip-coating method as described previously [25]. In this method, a sol is prepared from pseudoboehmite (AlOOH, Pural from Sasol), urea and 0.3 M nitric acid with a weight ratio of 2:1:5. After stirring for 24 h, the dried monolith is dipped in this sol for few minutes until all air bubbles inside the channels are removed. Subsequently, the monolith is withdrawn from the sol and the liquid inside the channels is removed by flushing thoroughly with pressurized air and then dried at room temperature for 24 h, while continuously being rotated around its axis. Finally, the monolith is calcined in air at a rate of 1 K/min up to 873 K, and this temperature is kept for 2 h to obtain the γ-alumina washcoating. The as-prepared monolith weighted ca. 2.6 g and the alumina content amounted to ca. 6 wt.% of the monolith weight. Subsequently, nickel was deposited by adsorption from pH-neutral nickel solution as described previously [25]. The monolith samples were kept (vertical position) 24 h in this solution while continuously flowing Ni solution through them. After that time, the monoliths were rinsed thoroughly with deionised water, followed by drying first at room temperature overnight and later calcined in flowing nitrogen (100 mL/min and 1 K/min) up to 873 K followed by 2 h dwell time. The nickel content was analysed by inductive coupled plasma optical emission spectroscopy (ICP-OES). In all cases, the nickel loading was ca. 15 wt.% of alumina washcoating. The preparation method is reproducible within ±5% experimental error.

In parallel, a sol of the alumina similar to that used to coat the monoliths was cured and calcined at the same conditions as explained above for the alumina sol coating the monoliths. The γ-alumina powders were ground and sieved to particles smaller than 200 μm. Subsequently, Ni was impregnated by electrostatic adsorption with a pH-neutral Ni solution during 24 h under stirring, i.e. in conditions similar to those used for impregnating the monoliths. Subsequently, the Ni-impregnated Al_2O_3 powder was rinsed thoroughly with deionised water, followed by drying first at room temperature overnight and later calcined in flowing nitrogen (100 mL/min and 1 K/min) up to 873 K followed by 2 h dwell time. This catalyst was also tested in ammonia decomposition in fixed bed and it was denoted as un-supported Ni/Al_2O_3.

2.2. Catalytic testing

Catalyst reactivity system consists of a continuous-flow 15 mm i.d. quartz reactor inside horizontal furnace with a temperature controller (Eurotherm). The monolithic nickel catalyst was wrapped with quartz stripe and it was tightly fitted to the wall of the quartz reactor to avoid channelling. Subsequently, the reactor was placed in the constant temperature zone of the furnace. The reaction testing was carried out after catalyst reduction in hydrogen atmosphere (100 ml/min H_2:N_2, 50:50) at 823 K for 1 h. The feed gas used for catalyst testing was anhydrous ammonia. The flow rates of the gases were fixed with Bronkhorst mass flow controllers. The catalysts were tested between 573 and 973 K. The outlet reaction gases were analysed with an Agilent Micro GC 3000A. H_2 an N_2 were analysed in a molsieve column and ammonia in a Plot-Q column. To ensure repeatability, 2–3 separate GC samples were taken and averaged for each experimental data point, and analyses were typically within ±3% of each other. The conversion was calculated taking into account the variations in the flow due to the mole increase in the reaction.

A sample of monolithic catalyst was additionally crushed and sieved to particle size smaller than 200 μm. The particles were packed in a fixed bed within a reactor of the same diameter as that used for the monoliths (15 mm i.d), giving rise to a bed height of 15 mm. The catalytic packed bed was tested under the same reaction condition that the structured catalyst to determine the role of geometrical catalyst configuration.

The particles of un-supported Ni/Al_2O_3 (size <200 μm) were also tested in fixed bed. The amount of un-supported Ni/Al_2O_3 catalyst in the bed was set the same as the amount of Ni/A_2O_3 catalyst coating the monolith. To keep the same bed height as for the bed of particles of crushed monolith, the particles of un-supported Ni/Al_2O_3 catalyst were mixed with SiC particles, which is known to have a high thermal conductivity. Therefore, the amount of alumina-supported catalyst is the same in all the experiments and the bed height is the same in all the packed bed experiments, i.e. 1.5 cm.

2.3. Catalyst characterization

The specific surface area was determinate by N_2 adsorption by the BET method in the relative pressure range 0.01–0.10 following the ASTM-4365 standard on a Micromeritics ASAP 2020 at 77 K. The pore size distribution was estimated by the BJH (Barrett–Joyner–Halenda) method from the adsorption branch. Transmission electron microscopy (TEM) images were obtained using a JEOL 2010F electron microscope equipped with a field emission gun. TEM specimens were prepared by ultrasonic dispersion in ethanol of powder retrieved from the monoliths. Temperature programme reduction (TPR) was carried out in a Micromeritics AutoChem II 2920. In TPR experiments, the catalyst was heated in 50 STPml/min of 10% H_2 in Ar at a rate of 10 K/min up to 1273 K. XRD diffractograms were recorded using a Bruker AXS D8ADVANCE diffractometer, in a θ–θ configuration and with a nickel-filtered Cu Kα radiation. The Ni content of the catalysts was analysed by ICP-OES after digestion of the samples in HCl.

The catalyst stability was checked by carrying out five cycles of reduction, reaction and cooling down with intermediate step of environmental exposure, amounting to a total of 30 h of operation at different temperatures. Finally, a heat treatment for 14 h at 923 K was carried out to assess the long-term stability at high temperature.

3. Results

3.1. Characterization of catalysts

Fig. 1 shows the N_2 adsorption isotherm of Ni on alumina washcoated monoliths and unsupported Ni on alumina catalyst. For comparison, also the isotherm of alumina wascoated monolith is displayed. The inset in Fig. 1 shows the pore size distribution (PSD). The mean pore size of alumina, between 4 and 5 nm, did not change after nickel deposition. Additionally, the BET specific surface area and pore volume increases from 200 $m^2\,g^{-1}$ and 0.26 $cm^3\,g^{-1}$ in the alumina washcoated monolith to 258 m^2/g and 0.36 $cm^3\,g^{-1}$ after nickel deposition. Both samples are mainly mesoporous with the microporosity only accounting for 13 and 15 $m^2\,g^{-1}$, respectively. Therefore, the mesopores of alumina are not plugged after Ni deposition suggesting that nickel particles are very uniformly distributed on the surface of alumina as small crystallites, decorating the edges of alumina pores or embedded in the alumina matrix. The reason of the increase of mesopore volume in the sample after Ni impregnation is uncertain. Anyway, these differences in surface area are not deemed significant because they lie within the experimental errors introduced in the determination of surface area.

Table 1 shows a comparison of the textural parameters of Ni/Al_2O_3 monoliths and un-supported Ni/Al_2O_3. Both catalysts have comparable surface areas and pore volumes. However, the mean pore size as determined by BJH pore size distribution (inset in Fig. 1 and Table 1) is ca. 1 nm smaller in the case of un-supported Ni/Al_2O_3. Shrinkage of the alumina takes place during calcinations. This process is less hindered for the un-supported Ni/Al_2O_3 than for the Al_2O_3 layer coating the monolith. The higher freedom of shrinkage for the former can account for its smaller mean pore size. Table 1 also shows the Ni loading for Ni/Al_2O_3 monolith and un-supported Ni/Al_2O_3 particles. The Ni loading on Al_2O_3 is higher in the monolith than in the powder particles despite that the preparation method by Ni electrostatic adsorption was the same for both catalysts. It is reasonable to assume that the smaller mean pore size and larger diffusion path in the un-supported Ni/Al_2O_3 particles (200 μm diameter) compared with the monoliths prevent the Ni precursor to diffuse to the inner core of un-supported Ni/Al_2O_3 particles. In contrast, the diffusion of Ni is favoured in the wider pores of the ca. 2 μm-thick alumina layer coating the monoliths, leading to higher Ni loadings.

Fig. 2 shows representative TEM images of catalysts after use, viz. figures (a) and (b) of the Ni/Al_2O_3 monolith catalyst and figures (c) and (d) of the un-supported Ni/Al_2O_3 particles. In Fig. 2a, the EDX analysis of revealed that the bottom part is cordierite, while the upper part is Ni dispersed on alumina. The dots of darkest contrast are Ni nanoparticles. The alumina is densely populated with Ni nanoparticles, which are very close one from another but they are still discrete. These Ni particles keep a small size after reaction. A statistical analysis revealed that the particle size distribution is log–normal with an average diameter of 6 nm (inset in Fig. 2a and c). The Ni particle size is comparable in both Ni/Al_2O_3 monolith and un-supported Ni/Al_2O_3. Therefore, alumina prevents the Ni nanoparticles to agglomerate despite the high temperature treatment (873 K) in reducing atmosphere. Fig. 2b shows a detail of the Ni particles in Ni/Al_2O_3 monolith. Lattice fringes can be observed in a Ni particle at the centre of the image. The particles are surrounded by a thin oxide coating, presumably formed during the exposure to air after reaction, which is confirmed below by TPR results. In un-supported Ni/Al_2O_3 catalyst, we did not observed the lattice fringes of Ni but we observed the lattice fringes of alumina embedding the Ni particle (Fig. 2d), pointing out to a strong metal-support interaction. By XRD (supporting information), no diffraction peaks were detected for all the catalyst, which can be due to several reasons such as the amorphous nature after reoxidation at ambient conditions, or the low Ni concentration due to the

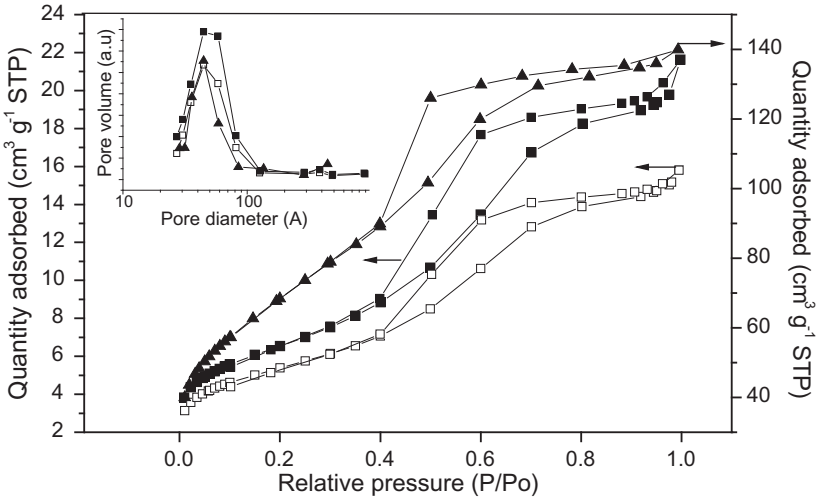

Fig. 1. N_2 adsorption/desorption isotherms of alumina-coated monolith (□), Ni on alumina coated monolith (■), and un-supported Ni/Al_2O_3 (▲). The inset shows the pore size distribution calculated applying the BJH method to the adsorption isotherm.

Table 1
Comparison of textural parameters and Ni particle size of Ni/Al_2O_3 monoliths and un-supported Ni/Al_2O_3.

Catalyst	Surface area (m^2/g)	Pore volume (cm^3/g)	Mean pore diameter[a] (nm)	Ni loading on alumina (%)	Mean Ni particle size[b] (nm)
Ni/Al_2O_3/monolith	258	0.36	4.5	15.0	6
Un-supported Ni/Al_2O_3	246	0.21	3.6	3.3	6.5

[a] Determined by BJH pore size distribution of N_2 adsorption in Fig. 1.
[b] Determined from TEM.

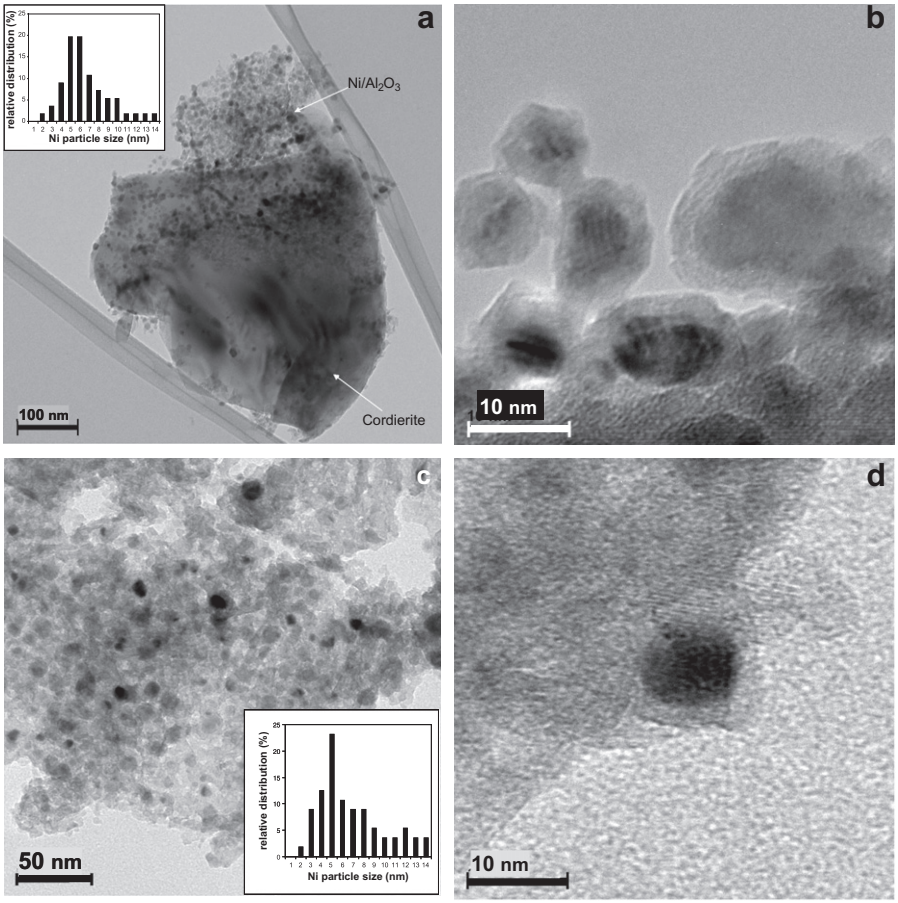

Fig. 2. Representative TEM image of the catalysts after use in NH_3 decomposition. (a and b) TEM images of Ni/Al_2O_3 monolith: (a) image showing the cordierite of the monolith at the bottom and Ni nanoparticles (darkest dots) on γ-alumina at the top, (b) detail of Ni nanoparticles; (c and d) TEM images of un-supported Ni/Al_2O_3.

dilution with cordierite, or to the superposition of Al_2O_3 or cordierite diffraction peaks.

The TPR of the used Ni/Al_2O_3 monolith catalyst exhibits only one peak at 460 K (Fig. 3). This means that Ni nanoparticles are reoxidised partially after air exposure but they are readily re-reduced at low temperature in H_2. The layer of Ni oxide can be observed in TEM images (Fig. 2b). On the contrary, the un-supported Ni/Al_2O_3 catalyst does not exhibit any reduction peak indicating that it was not reoxidised upon air exposure, which could be related to a stronger metal–support interaction. The absence of reduction peak at higher temperatures rules out the formation of refractory aluminates.

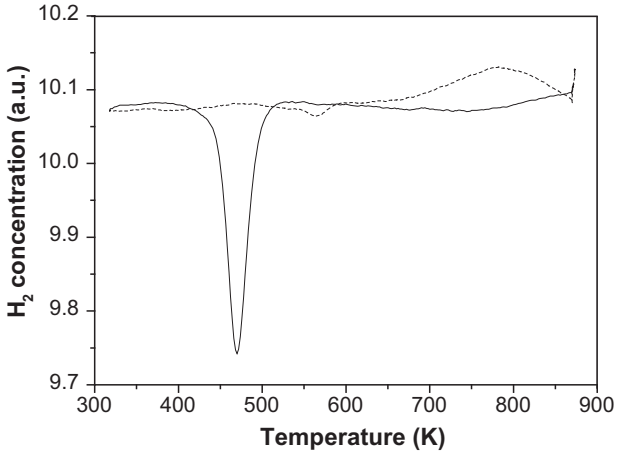

Fig. 3. Temperature programmed reduction of catalysts after reaction: Ni/Al_2O_3/cordierite monolith (solid line) and Ni/Al_2O_3 un-supported (dashed line).

3.2. Influence of the experimental conditions and catalyst configuration in NH_3 decomposition

We calculated the thermodynamic equilibrium NH_3 conversions for different ammonia concentrations using the software HSC chemistry-Outotec (Supplementary material). For pure ammonia, thermodynamic calculations show that the equilibrium NH_3 conversion is 100% at 650 K. In our catalytic test, the light-off temperature is around 700 K. Thus, our experiments are far from equilibrium limitations, and the reverse reaction can be neglected.

Fig. 4 illustrates the dependence of the conversion on the NH_3 concentration in the feed gas. The curve shifts to higher temperatures when the NH_3 concentration increases. In addition, as the concentration increases, the gap between the curves becomes narrower. The significantly higher conversions with diluted NH_3 suggest that the monolithic catalyst can be applied not only to produce H_2 from concentrated NH_3 but also to remove residual traces of NH_3. In this later case, it is possible to operate at about 100 K lower temperatures compared with the concentrated NH_3 decomposition, at least when the diluting gas is inert gas. To shed some light about the possible reason of this variation of the conversion with NH_3 concentration, we performed the experiment with 5% NH_3 but, instead of diluting in argon, we diluted in the products

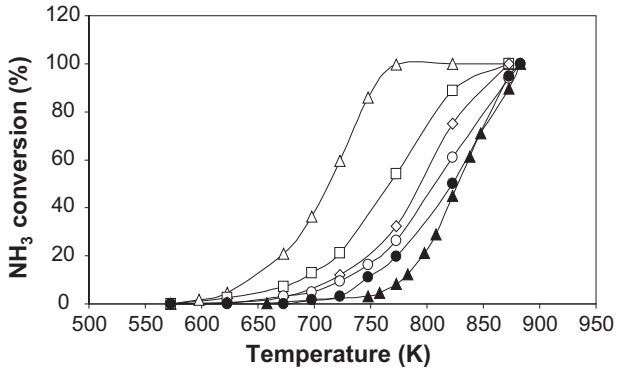

Fig. 4. Light-off curves of NH_3 decomposition with Ni/Al_2O_3 monolith using as gas feed 100 ml/min of different gas compositions. Several NH_3 concentrations diluted in argon: (△) 5% NH_3 in Ar, (□) 25% NH_3 in Ar, (◇) 50% NH_3 in Ar, (○) 75% NH_3 in Ar; pure ammonia (●) 100% NH_3; 5% NH_3 diluted in the product gases: (▲) 5% NH_3, 23.75% N_2 and 71.25% H_2.

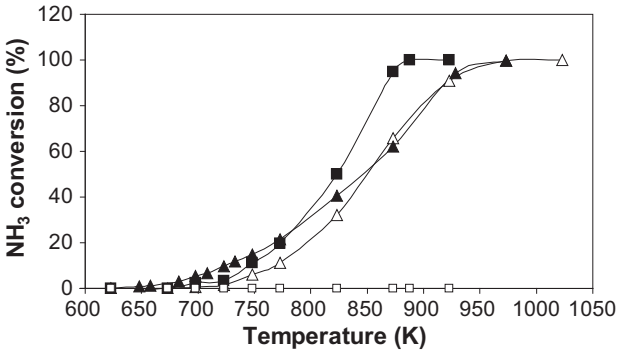

Fig. 6. Comparison of the light-off curves of the catalysts conformed to different spatial configurations: (□) blank experiment with Al_2O_3-coated cordierite monolith, (■) Ni/Al_2O_3-coated cordierite monolith, (△) bed of Ni/Al_2O_3-coated cordierite monolith crushed to particles smaller than 200 μm, (▲) bed of un-supported Ni/Al_2O_3 particles smaller than 200 μm. Total flow: 100 ml/min of pure NH_3.

of reaction in a ratio N_2:H_2 equal to 1:3, simulating the gas after 95% conversion of pure ammonia. Fig. 4 shows that, keeping constant the NH_3 concentration (5%), the conversion is substantially lower in the presence of the reactions products. We substituted N_2 by Ar keeping the same H_2 percentage, and there is no difference in the conversion curve, demonstrating that the inhibition is caused by H_2. The inhibition by H_2 has already been reported in the literature [7]. This explains the shift of the light-off curve to higher temperatures when the NH_3 concentration in the feed gas increases. When the feed NH_3 concentration is higher for a constant conversion, the amount of H_2 produced is higher and thus the inhibition of reaction is more pronounced.

For application to on-site H_2 generation, it is desirable to use pure ammonia as feed. Fig. 5 shows the dependence of the conversion on the flow rate of pure NH_3. When the flow rate increases, the curve shifts to slightly higher temperatures. The highest flow rate tested in this work is 100 ml/min, which corresponds to a GHSV of 35,000 $cm^3\ g^{-1}\ h^{-1}$ referred to the grams of Ni/Al_2O_3 catalyst. This is considered a sufficiently high space velocity for a real application.

Fig. 6 displays conversion curves for decomposition of 100 ml/min of NH_3 using catalysts based on Ni/γ-Al_2O_3 conformed in different configurations, viz. (i) the Ni/Al_2O_3-coated cordierite monolith, (ii) the packed bed formed by the monolithic catalyst but crushed to particles smaller than 200 μm and (iii) the packed bed formed by particles of un-supported Ni/A_2O_3 smaller than 200 μm. It is noteworthy that the amount of Ni/Al_2O_3 catalyst is the same in the three cases. The blank experiment indicated that the alumina-coated monolith is inactive in the temperature range tested.

Comparing the monolithic catalyst and the bed of the same catalyst but smashed to particles, the monolith outperforms the packed bed in all the temperature range, despite that the catalyst is the same and only the configuration changes. Additionally, the Ni/A_2O_3 monolithic catalyst also outperforms the bed of un-supported Ni/A_2O_3 particles, achieving total conversion at about 100 K lower temperature. Although at low temperatures, i.e. lower than 800 K, the bed of un-supported Ni/Al_2O_3 catalyst has slightly higher conversion, and at medium and high temperatures, the performance of the monolith exceeds that of un-supported Ni/Al_2O_3 catalyst bed. The lower conversion of un-supported Ni/Al_2O_3 at high temperatures can be attributed to the lower Ni loading and to internal diffusion limitations. Internal diffusion may become rate-limiting at high temperatures for un-supported Ni/Al_2O_3 particles, which have a diffusion path around 100 μm versus about 2 μm for the Ni/Al_2O_3 coating on the monolith.

In order to check the stability of the catalyst, we carried out five cycles of reduction, reaction at different temperatures and exposition to air, amounting to a total of 30 h of operation. Subsequently, the same catalyst was maintained for 14 h at 923 K, to determine the effect on the stability of long-term exposition to the temperature

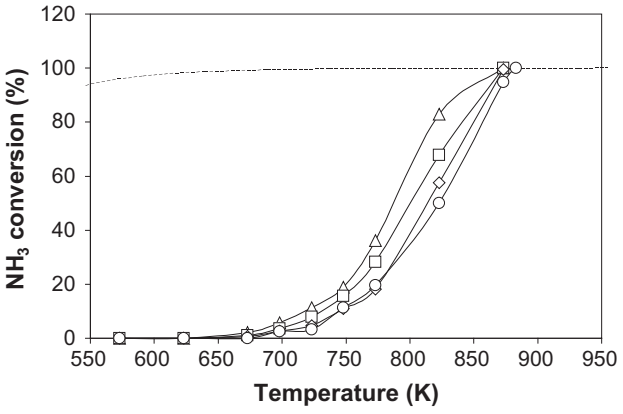

Fig. 5. Light-off curves of NH_3 decomposition with Ni/Al_2O_3 monolith for different feed flow rates of pure NH_3: (△) 25 ml/min, (□) 50 ml/min, (◇) 75 ml/min, (○) 100 ml/min. The dotted line represents the equilibrium conversion.

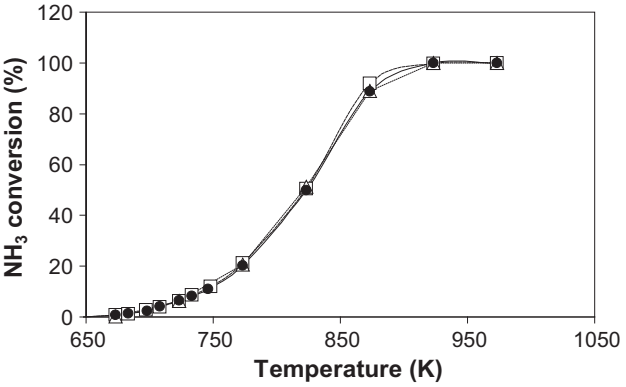

Fig. 7. Stability tests with Ni/Al_2O_3-coated monoliths. (□) conversion in initial run, (△) conversion after five cycles of reduction, reaction and cooling down with environmental exposure, amounting to a total of 30 h of operation at different temperatures; (●) conversion after subsequent heat treatment for 14 h at 923 K. Total flow: 100 ml/min of pure NH_3.

of complete conversion. The results of the stability tests are shown in Fig. 7. It can be observed that conversion did not change, which indicates that the structured catalyst showed excellent stability under cyclic reduction–reaction–air exposure conditions and under long period of heat treatment.

4. Discussion

The exact reason of the higher conversion of the monolithic catalyst respect to the packed bed is not completely unravelled. Several factors may cooperate for the better performance of monolith. We can put forward some hypothesis such as the better flow distribution for the monolith with no catalyst bypassed by the gas or no dead volumes, which are more likely to occur in packed beds. The heat transmission may also play a role in an endothermic reaction as NH_3 decomposition. The heat is transmitted faster in a monolithic structure than in a bed of unconnected particles. The thermal transmission in the bed of un-supported Ni/Al_2O_3 diluted with SiC (a good heat conductor) and of the entire monolith is presumably faster than that of the crushed monolith bed. In an endothermic reaction, when the heat transfer is faster, the probability of formation of colder spots decreases and hence conversion may increase. Another hypothesis is that the inhibiting effect of produced H_2 is minimised in the monolith. The shorter diffusion paths and absence of dead volumes in the monolith make that H_2 and N_2 are removed more readily from the catalytic sites by the flowing gases. The fact that the differences in conversion between monoliths and packed beds increase in parallel with conversion supports the hypothesis of the faster heat transmission and better removal of inhibitor H_2 in the monolith. The conversions of monolith and packed beds are comparable at the low conversion range, where lower amount of produced H_2 and heat are involved. When conversion increases, the inhibition by H_2 and the heat involved is more relevant and hence the difference in conversion between monolith and fixed beds increases.

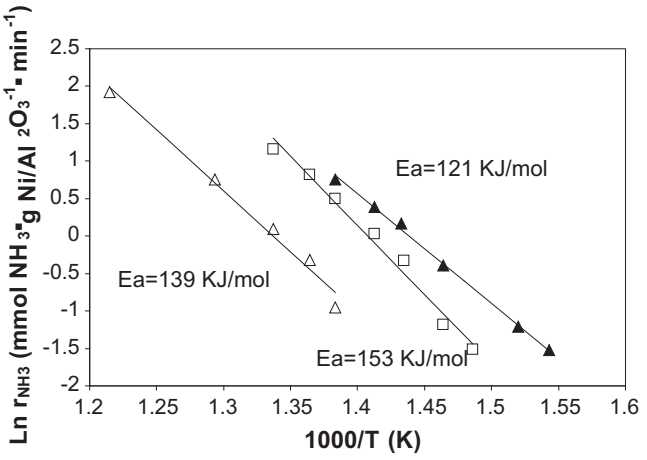

Fig. 8. Logarithm of ammonia decomposition rate as a function of inverse temperature for ammonia conversions between 3% and 20% in experiments carried out with 100 ml/min of pure NH_3. Catalyst configurations: (□) Ni/Al_2O_3-coated cordierite monolith, (△) bed of Ni/Al_2O_3-coated cordierite monolith crushed to particles smaller than 200 μm, (▲) bed of un-supported Ni/Al_2O_3 particles smaller than 200 μm.

Fig. 8 shows the Arrhenius plot for different reactor systems tested here, i.e. the monolith, bed of smashed monolith and un-supported Ni/Al_2O_3. The values of apparent activation energies were calculated for conversions between 3% and 20% to keep differential reactor conditions. At these low conversions, the catalyst of un-supported Ni/Al_2O_3 exhibited higher activity than the other catalysts in agreement with Fig. 6. Nevertheless, the activity of the monolithic catalyst is higher at conversions above 20%. The apparent activation energy varies between 120 and 150 kJ/mol. These values are larger than those reported in the literature for Ni on SiO_2/Al_2O_3 and HZSM-5, 84 and 92 kJ/mol, respectively [18]. However, they are lower than values reported for Ni wires (211 kJ/mol) [28]. The discrepancy of the activation energy values found here with the values of the literature for Ni/Al_2O_3 can stem from the different Ni particle size. A dependence of apparent activation energy with Ni particle size has been reported in the literature [27]. In that work, apparent activation energies comparable to this work (ca. 120 kJ/mol) were found for Ni particle size around 2.5 nm. The mean particle size determined here by TEM is 6 nm but the actual size is likely smaller because most of particles smaller than 3 nm are missed due to the poor contrast of these particles by TEM.

Although the major part of the works in the literature evidenced that Ruthenium is the most active metal, there are some few works in the literature underscoring the high activity of Ni catalyst in NH_3 decomposition [18,19]. However, as far as we know, there is no precedent in the literature testing Nickel catalyst supported on cordierite monoliths in NH_3 decomposition for H_2 generation. There are works using cordierite monoliths but they addressed the cleaning of diluted NH_3 streams [29].

Some works in the literature have performed the catalytic testing of ammonia decomposition using diluted NH_3 feeds and, in other works, the research did not address total conversion. Although these investigations are very interesting from fundamental research standpoint, these experimental conditions does not reproduce the ideal conditions for real application. The operation at nearly 100% conversion is desired for the implementation of this technology for in situ H_2 generation because it minimises the amount of absorbent needed for residual NH_3 removal. Different technological possibilities can be applied to increase the conversion to 100% such as working with recirculation or increasing the amount of catalyst. In our experiments, the Ni/Al_2O_3 monolithic reactor, in contrast to Ni/Al_2O_3 powdered catalysts, gives rise to 100% conversion of pure ammonia at 873 K. Therefore, neither other technological solution nor adsorbent should be implemented, reducing the cost of the process.

The dependence of the light-off curves with NH_3 composition (Fig. 4) and flow rate (Fig. 5) make difficult to withdraw general conclusions from literature results, taking into account that different NH_3 concentrations and flow rates are reported in the

Table 2
Experimental details of some selected catalysts in the literature.

ID	Catalyst	Amount catalyst (mg)	Flow rate STP (ml min^{-1})	Surface area of support (m^2)	Reference
1	0.8 wt.% Ru on N-CNT	100	70	–	[13]
2	1 wt.% Ni Al microreactor	–	92	25	[26]
3	65 wt.% $Ni/SiO_2/Al_2O_3$	100	50	–	[18]
4	10 wt.%Ru/SiO_2	100	50	–	[18]
5	3.5 wt.% Ru–0.8 wt.% K on Al microreactor	–	145	2.4	[8]
6	15 wt.% Ni/Al_2O_3-coated monolith	170	100	39.4	This work

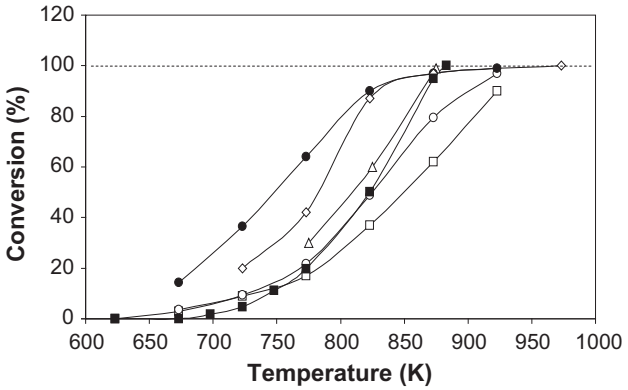

Fig. 9. Comparison of the light-off curves for several catalysts and microreactors tested in the literature using pure ammonia. (△) catalyst n° 1; (□) catalyst no. 2; (○) catalyst no. 3; (●) catalyst no. 4; (◇) catalyst no. 5; (■) catalyst prepared in this work.

literature. Table 2 and Fig. 9 show the comparison of selected catalysts from literature. We have left aside of this comparison catalysts tested with diluted NH_3 feed [9,10,14] because, as we showed above, gas feed of NH_3 diluted in inert gas led to higher conversion than pure NH_3 due to the lower inhibition caused by product H_2 in the former case. From Fig. 9, it is apparent that our catalyst has comparable conversion than catalyst no. 1, which is based on ruthenium supported on nitrogen-doped-CNT. It is reported that ruthenium is intrinsically more active than Ni but the higher amount of Ni in our catalyst and the enhanced mass/heat transfer properties of monolith seem to compensate for the higher specific activity of ruthenium.

Compared with those catalysts based on Ni, i.e. catalyst no. 2 and no. 3, the monolithic catalyst prepared here has similar conversions at low and medium temperatures but it outperformed them at high temperatures. The higher conversion of our catalyst with respect to catalyst no. 2 can be ascribed to the higher Ni loading and surface area of monolith with respect to 1% Ni on microreactor catalyst no. 2. On the other hand, the higher conversion of the monolith catalyst of this work compared with catalyst no. 3 (65% Ni) could be also attributed to the enhanced mass and heat transfer of the monolith relative to the powder catalyst.

The most active catalysts are those based on ruthenium, i.e. catalyst no. 4 and no. 5. This is especially evident at low and medium temperatures but at the highest temperatures, the differences with our Ni-based catalyst are blurred. Up to 80% conversion, the ruthenium catalysts nos. 4 and 5 have higher conversion than the monolithic catalyst here prepared. This could be explained in terms of the higher intrinsic activity of ruthenium. However, at conversions around 97%, the activity of the Ni/Al_2O_3 monolith prepared here compares with the ruthenium catalysts nos. 4 and 5. This could be explained by the enhanced heat and mass transfer of the monoliths compared to the powder catalyst no. 4 and to the higher surface area and, therefore, catalyst inventory of monolith compared with microreactor catalyst no. 5. It can be envisaged that a catalyst of Ru well dispersed on the alumina-coated monoliths can have a performance exceeding that of Ni/Al_2O_3 monolith.

The stability tests indicated that there is no Ni sintering during long-term experiments at temperature of 100% conversion (Fig. 7). A way to estimate the sintering temperature onset is through the T_{amman} and Hüttig temperature [30], where T_{Tamman} is the temperature at which atoms in the bulk will start to diffuse and $T_{Hüttig}$ is when atoms at defects will become mobile. These temperatures can be approximated by the following semi-empirical equation: $T_{Tamman} = 0.5 \times T_{melting}$ and $T_{Hüttig} = 0.3 \times T_{melting}$. At the reaction conditions used here, the reaction temperature needed to attain 100% NH_3 conversion is 873 K, which is greater than Hüttig temperature ($T_{Melting\ Ni} = 1726$ K; $T_{Hütting} = 518$ K) and very close to Tamman temperature ($T_{Tamman} = 863$ K). From the above results, we can conclude that the catalyst stability is due to the good metal-support interaction, which prevents the sintering of Ni nanoparticles. It has been reported that the support can prevent sintering by effect of physical hindrance. The pore structure and surface roughness of the support may affect the final size distribution of nickel particles and mainly their evolution during the reaction [31]. More recently, it has been reported that the bond strength between Ni and alumina is enhanced by strong Lewis acid sites of γ-alumina in low-coordinated alumina sites [32]. Therefore, we can attribute the good metal-support interaction in our catalytic system either to the textural properties or to the acidic properties of the Al_2O_3 support, which eventually prevents the sintering of Ni nanoparticles.

5. Conclusions

We have prepared, characterized and tested in NH_3 decomposition a structured catalytic reactor consisting of Ni supported on alumina-coated monoliths. The catalyst is based on a non-precious metal, thus cost-effective for a widespread application in H_2 generation. After prolonged reaction, the catalyst keeps Ni dispersed with particles of 6 nm mean size and mesopores between 4 and 5 nm. The nickel does not plug the mesopores and remains anchored within the alumina matrix. These features render a catalyst with high activity and stability in the reaction of NH_3 decomposition, achieving a 100% conversion of pure ammonia at 880 K. In comparison with packed bed of the same catalyst, monolith reactor configuration exhibits substantially higher conversions, has lower pressure drop and more robustness for mobile applications. Moreover, the NH_3 conversions are comparable to other catalysts and structured reactors reported in the literature, including ruthenium catalyst. The characterization and testing of the monolithic catalyst point out that it has good prospects to be used for in situ H_2 generation from ammonia decomposition.

Acknowledgments

We are grateful to the financial support of the Spanish Government (MAT 2008-02365, CTQ 2007-62545/PPQ) and of regional government (DGA-LACAIXA GA-LC-043/2010). S. Armenise also thanks the Santander bank for a doctoral fellowship. We are also grateful to David Villellas for his assistance in the laboratory.

Appendix A. Supplementary material

Supplementary data associated with this article can be found, in the online version, at doi:10.1016/j.jcat.2010.07.026.

References

[1] R. Socolow (Ed.), Fuels Decarbonization and Carbon Sequestration, Report No. PU/CEES 302, Princeton University Press, Princeton, September 1997, p. 17, 2010.
[2] C.H. Christensen, R.Z. Sorensen, T. Johannessen, U.J. Quaade, K. Honkala, T.D. Elmoe, R. Kohler, J.K. Norskov, Journal of Materials Chemistry 15 (2007) 4106.
[3] F.A. Uribe, S. Gottesfeld, T.A. Zawodzinski, Journal of the Electrochemical Society 149 (2002) A293–A296.
[4] http://www1.eere.energy.gov/hydrogenandfuelcells/pdfs/32405b15.pdf, 2007.
[5] O. Hinrichsen, F. Rosowski, A. Hornung, M. Muhler, G. Ertl, Journal of Catalysis 165 (1997) 33.
[6] Z.h. Zhong, K.i. Aika, Journal of Catalysis 173 (1998) 535.
[7] M.C.J. Bradford, P.E. Fanning, M.A. Vannice, Journal of Catalysis 172 (1997) 479.
[8] J.C. Ganley, E.G. Seebauer, R.I. Masel, Journal of Power Sources 137 (2004) 53.
[9] W. Pyrz, R. Vijay, J. Binz, J. Lauterbach, D. Buttrey, Topics in Catalysis 50 (2008) 180.

[10] R.Z. Sorensen, A. Klerke, U. Quaade, S. Jensen, O. Hansen, C.H. Christensen, Catalysis Letters 112 (2006) 77.
[11] W. Rarog-Pilecka, D. Szmigiel, Z. Kowalczyk, S. Jodzis, J. Zielinski, Journal of Catalysis 218 (2003) 465.
[12] S.J. Wang, S.F. Yin, L. Li, B.Q. Xu, C.F. Ng, C.T. Au, Applied Catalysis B: Environmental 52 (2004) 287.
[13] J. Chen, Z.H. Zhu, S. Wang, Q. Ma, V. Rudolph, G.Q. Lu, Chemical Engineering Journal 156 (2010) 404.
[14] F.R. García-García, J. Álvarez-Rodríguez, I. Rodríguez-Ramos, A. Guerrero-Ruiz, Carbon 48 (2010) 267.
[15] S.F. Yin, Q.H. Zhang, B.Q. Xu, W.X. Zhu, C.F. Ng, C.T. Au, Journal of Catalysis 224 (2004) 384.
[16] S.F. Yin, B.Q. Xu, X.P. Zhou, C.T. Au, Applied Catalysis A: General 277 (2004) 1.
[17] S.T. Oyama, Journal of Catalysis 133 (1992) 358.
[18] T.V. Choudhary, C. Sivadinarayana, D.W. Goodman, Catalysis Letters 72 (2001) 197.
[19] J.C. Ganley, F.S. Thomas, E.G. Seebauer, R.I. Masel, Catalysis Letters 96 (2004) 117.
[20] A.S. Chellappa, C.M. Fischer, W.J. Thomson, Applied Catalysis A: General 227 (2002) 231.
[21] J. Zhang, J.O. ller, W. Zheng, D. Wang, D. Su, R. Schlogl, Nano Letters 8 (2008) 2738.
[22] S.R. Deshmukh, A.B. Mhadeshwar, D.G. Vlachos, Industrial and Engineering Chemistry Research 43 (2004) 2986.
[23] Christian, M. Mitchell, D.P. Kim, P.J.A. Kenis, Journal of Catalysis 241 (2006) 235.
[24] T.A. Nijhuis, A.E.W. Beers, T. Vergunst, I. Hoek, F. Kapteijn, J.A. Moulijn, Catalysis Reviews – Science and Engineering 43 (2001) 345.
[25] E. Garcia-Bordeje, I. Kvande, D. Chen, M. Ronning, Carbon 45 (2007) 1828.
[26] J.C. Ganley, K.L. Riechmann, E.G. Seebauer, R.I. Masel, Journal of Catalysis 227 (2004) 26.
[27] J. Zhang, H. Xu, W. Li, Applied Catalysis A: General 296 (2005) 257.
[28] R.W. McCabe, Journal of Catalysis 79 (1983) 445.
[29] Z.R. Ismagilov, R.A. Shkrabina, S.A. Yashnik, N.V. Shikina, I.P. Andrievskaya, S.R. Khairulin, V.A. Ushakov, J.A. Moulijn, I.V. Babich, Catalysis Today 69 (2001) 351.
[30] J.A. Moulijn, A.E. van Diepen, F. Kapteijn, Applied Catalysis A: General 212 (2001) 3.
[31] P. Desai, J.T. Richardson, in: B. Delmon, C.G. Froment (Eds.), Catalyst Deactivation, Elsevier Science Publishing Company, Amsterdam, 1980, p. 149.
[32] J. Lif, I. Odenbrand, M. Skoglundh, Applied Catalysis A: General 317 (2007) 62.